RESEARCH ARTICLE

NANO · MICRO small
www.small-journal.com

Cyclic Ether-Based Electrolyte with a Weak Solvation Structure for Advanced Potassium Metal Batteries

*Danni Wang, Zhijie Wang, Dengyun Zhai, and Biao Zhang**

Potassium metal batteries (PMBs) are promising candidates for large-scale energy storage. Conventional carbonate electrolytes exhibit unsatisfactory thermodynamic stability against potassium (K) metal anode. Linear ether is widely adopted because of its compatibility with K metal, but the poor oxidation stability restricts the application with high-voltage cathodes. Herein, a weakly solvating cyclic ether is proposed as a solvent to stabilize the K-electrolyte interface and build a robust solid-electrolyte interphase (SEI). This weakly solvating electrolyte (WSE) possesses an anion-dominated solvation structure, which facilitates the anion decomposition for constructing an inorganic-rich SEI. The superior mechanical properties of the SEI, as examined by atomic force microscopy, prevent the SEI from fracture. Consequently, this WSE achieves highly reversible plating/stripping behavior of K metal for 1300 h with a high average Coulombic efficiency of 99.20%. Stable full cells are also demonstrated with a high-voltage cathode at harsh conditions. This work complements the design of WSEs for advanced PMBs by cyclic ether solvents.

1. Introduction

Lithium (Li)-ion batteries (LIBs) have been extensively applied to many aspects of modern society, but they are still faced with several challenges, such as Li resource scarcity and uneven distribution in the earth's crust.[1] Sodium (Na)-ion batteries and potassium (K)-ion batteries (PIBs) have emerged as attractive candidates to LIBs.[2] Compared with Na^+/Na (−2.71 V versus the standard hydrogen electrode (SHE)), K^+/K (−2.93 V vs SHE) is closer to Li^+/Li (−3.04 V vs SHE), suggesting that it is more likely to achieve higher potential for enhanced energy density in PIBs.[3] Among the various reported anode materials, the direct use of K metal anode is a promising choice, owing to its lowest electrochemical potential and highest theoretical specific capacity of 687 mAh g^{-1}.[4] Admittedly, there are some problems with K metal anode, including large volume variation, unstable solid-electrolyte interphases (SEIs), and uncontrollable growth of K dendrite.[1c,5] The SEI formed on the K metal anode under conventional carbonate electrolytes shows poor interfacial stability and mechanical properties, reducing the K reversibility and shortening its lifespan.[6] The chemical composition of SEIs and the interfacial stability are highly related to electrolyte formulations.[7] Hence, it is vital to develop suitable electrolytes to stabilize potassium metal batteries (PMBs).

Most of the explorations about electrolytes for PMBs are based on ether electrolytes because of their better reduction stability against the K metal anode.[8] In 2017, Wu's group reported the reversible plating/stripping behavior of K metal in potassium bis(fluorosulfonyl)imide (KFSI)/dimethoxyethane (DME) electrolyte for the first time.[4a] Nevertheless, the poor anodic stability of diluted KFSI/DME electrolytes limited its further application. Kang's group proposed a highly concentrated electrolyte (HCE), 4 M KFSI/diethylene glycol dimethyl ether, realizing stable cycling of K metal anode with a high Coulombic efficiency (CE) over 98%.[1b] The HCE can improve the oxidation stability of electrolytes significantly, and lead to anion-derived interfacial chemistry. However, it possesses some shortages, including high cost, high viscosity, and poor wettability. To overcome these disadvantages, some non-solvating diluents are introduced into HCE to generate a localized highly concentrated electrolyte (LHCE).[7a,9] Recently, Xie's group introduced 1,1,2,2-Tetrafluoroethyl-2,2,3,3-tetrafluoro-propyl ether into KFSI/DME electrolyte to obtain a LHCE.[10] It facilitated the formation of a robust and stable SEI on the K metal anode, achieving an anode-free full cell. In addition, 1,2-diethoxyethane was reported as a weakly solvating solvent to weaken the K^+-solvent interaction, regulating the interfacial chemistry.[11] With a moderate concentration of 2 M, the electrolyte realized a high average CE of 98.9% in K||Cu batteries. As another pathway to access the anion-derived

D. Wang, Z. Wang, B. Zhang
Department of Applied Physics and Research Institute for Advanced Manufacturing
The Hong Kong Polytechnic University
Hung Hom, Hong Kong 999077, China
E-mail: biao.ap.zhang@polyu.edu.hk
D. Zhai
Shenzhen Geim Graphene Center
Institute of Materials Research
Tsinghua Shenzhen International Graduate School
Tsinghua University
Shenzhen 518055, China

The ORCID identification number(s) for the author(s) of this article can be found under https://doi.org/10.1002/smll.202403642

DOI: 10.1002/smll.202403642

interfacial chemistry, weakly solvating electrolyte (WSE) can reduce the desolvation energy, improve the plating kinetics of alkali metal, and build an inorganic-rich interphase at low concentrations to decrease the cost.[8] However, the existing research about WSEs for PMBs is insufficient and necessitates deep investigation.

In this work, we design a novel WSE to achieve an anion-derived interfacial regulation and decent electrochemical performances. It is formulated by dissolving KFSI into a cyclic ether, 1,3-dioxane (1,3-DX). The intrinsically weak solvating power of the solvent results in the anion-dominated solvation structure, which leads to the formation of anion-derived inorganic-rich SEIs with a high maximum elastic deformation energy on the K metal anode. Consequently, the plating/stripping of K metal presents an attractive average CE of 99.20%, with a long lifetime of 1300 h at a current density of 0.5 mA cm^{-2}. Additionally, it can improve the oxidation resistance of the electrolyte. The full cell with a Prussian blue cathode delivers capacity retention of 84.1% after 100 cycles under a negative/positive capacity ratio of 5.

2. Results and Discussion

2.1. Physical Properties of Solvents and Electrolytes

The 1,3-DX has an advantage in physical properties over the common cyclic and linear ether solvents. As shown in Table S1 (Supporting Information), the 1,3-DX has the highest boiling and flash points compared with the widely used three ether solvents with similar molecular structure, suppressing the thermal evaporation of electrolyte. The electrolyte is formulated by dissolving KFSI into the 1,3-DX with a regular concentration of 1 M. Since the normal ether, such as DME, is not compatible with high voltage cathode (as discussed later), the conventional carbonate electrolyte, 1 M KFSI in ethylene carbonate (EC)/ diethyl carbonate (DEC) (1:1 vol), is examined for comparison. These two electrolytes are denoted as E@1,3-DX and E@EC/DEC, respectively. Some important properties of the two electrolytes are also measured as listed in Table S2 (Supporting Information). The E@1,3-DX shows superiorities on viscosity, density, frozen point, and K^+ transference number. Its lower ionic conductivity could be attributed to the weaker solvation, which will be discussed later.

2.2. Solvation Structure of Electrolytes

Nuclear magnetic resonance (NMR) spectroscopy was collected to reveal the chemical environments around C and F atoms in the electrolytes. The coordinating atom with the cation in a solvent is usually the O atom. Therefore, the C atoms directly bonding with the coordinating O should be focused on. **Figure** 1a shows the peaks of C atom a and b (b') in the E@1,3-DX exhibit upfield shifts, owing to the solvation.[12] As for carbonate solvents, in Figure S1 (Supporting Information), the peaks of the carbonyl carbons in EC and DEC have downfield shifts, suggesting the K^+-solvent interaction in E@EC/DEC.[13] Hence, the degree of solvation can be figured out through the comparison of changes of the chemical shift. The chemical shift change for EC is more than that for the 1,3-DX. Note that the less shift change for DEC is related to the preferential coordination of EC with K^+.[13] Thus, it can be inferred that the solvation is weaker in the E@1,3-DX. Furthermore, according to the ^{19}F NMR spectra in Figure 1b, the peak of the E@1,3-DX has a downfield shift compared with that of the E@EC/DEC, which indicates that F atoms in the E@1,3-DX have lower electron density resulting from the stronger interaction between FSI^- and K^+ owing to the weak solvation.[14]

The distinction of solvation structures was further investigated by Raman spectroscopy (Figure 1c). The Raman signals between 685–775 cm^{-1} originate from the S-N-S stretching mode in the FSI^- anion.[15] It is noted that EC also has signals in this shift range, i.e., 717.06 cm^{-1} for free EC (Figure S2, Supporting Information) and 721 cm^{-1} for EC binding with K^+.[16] It shows that the major part of the E@EC/DEC is solvent-separated ion pairs (SSIPs, 719 cm^{-1}). In contrast, the solvation structure is dominated by contact ion pairs (CIPs, 729.6 cm^{-1}) and ion aggregates (AGGs, 740.3 cm^{-1}) in the E@1,3-DX (Figure 1d), reflecting the weaker solvation capability of the 1,3-DX. For the completeness of our studies, we also compare it with the solvation structure of classical linear ether-based electrolytes, i.e., 1 M KFSI/DME (E@DME, Figure S3, Supporting Information). The E@1,3-DX presents a weaker solvation than E@DME, evidenced by the higher proportion of AGG and less SSIP. In short, these NMR and Raman results demonstrate that the solvation structure in the E@1,3-DX is anion-dominated owing to the weak solvation capability of the solvent 1,3-DX.

2.3. Electrochemical Performance and Morphology of K Metal Anode

K||carbon-coated Al (Al-C) cells were tested to evaluate the reversibility of K plating/stripping in different electrolytes. As shown in **Figure** 2a, the average CE is 99.20% in the E@1,3-DX, which is among the highest values achieved in the PMBs (Table S3, Supporting Information). In particular, the electrolyte is made of a solo salt and a solo solvent under a normal concentration of 1 M, simplifying the fabrication process. Besides, the significantly higher initial CE (ICE) of 96.64% in the E@1,3-DX means less decomposition of the electrolyte at the initial stage.[1b,17] Meanwhile, the lifespan of K||Al-C cell in the E@1,3-DX is also much longer (1300 h) than that in the E@EC/DEC (197 h) (Figure S4, Supporting Information). Under a smaller current density (0.25 mA cm^{-2}), the performances of both electrolytes become more stable, due probably to less uncontrollable dendrite growth (Figure S5a, Supporting Information). Accordingly, the average CEs are improved to 99.22% and 98.59% for E@1,3-DX and E@EC/DEC, respectively. As for a higher current density and a larger areal capacity (1 mA cm^{-2}, 2 mAh cm^{-2}) (Figure S5b, Supporting Information), the ICEs of both electrolytes decrease but the average CE in the E@1,3-DX remains to be over 99%, while a lower value of 97.18% is observed in the E@EC/DEC.

The voltage profiles of K||Al-C cells in the two electrolytes were also investigated (Figure 2b). The E@1,3-DX exhibits lower nucleation overpotential than that of the E@EC/DEC, implying the former establishes a preferable environment for the nucleation of K^+ by reducing the nucleation barrier.[10] This could benefit the initial deposition for achieving a remarkable ICE.[18] Turn-

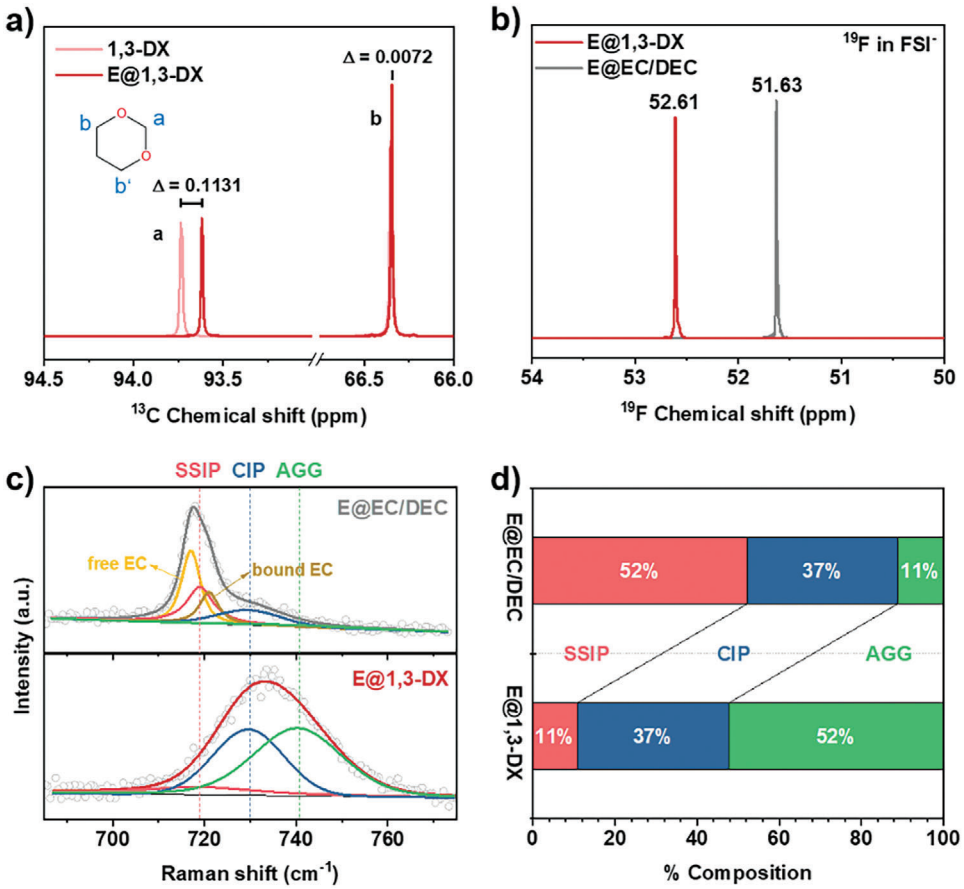

Figure 1. Characterizations of solvation structure in two electrolytes. a) ^{13}C NMR spectra of the pure solvent 1,3-DX and the electrolyte E@1,3-DX. Inset shows the molecular structure of the 1,3-DX. b) ^{19}F NMR spectra of the E@1,3-DX and the E@EC/DEC. c) Raman spectra of the E@1,3-DX and the E@EC/DEC, which are deconvoluted for different components in solvation structures. d) The proportions of different coordination states of FSI^- in the two electrolytes.

ing to the overall overpotential of cells during the first cycle, a high value is detected in the E@1,3-DX. Nevertheless, the overpotential becomes smaller after ten cycles, as depicted in the bottom of Figure 2b. We also measured the CE through the Aurbach method,[19] where the cell shows a value of over 98% under the E@1,3-DX (Figure S6, Supporting Information). In comparison, short circuit takes place under the E@EC/DEC before completing the test. In addition, K||K symmetric cells were also tested. As shown in Figure 2c, the K||K cells in the E@1,3-DX are facile to achieve a long cycling life of over 500 h, which is over three times that in the E@EC/DEC. This suggests the growth of K dendrites is suppressed in the E@1,3-DX, and the possibility of an internal short circuit is reduced. The rate performance of K||K cell in the E@1,3-DX is also attractive as it can stand a considerable current density of 2 mA cm^{-2}, followed by stable cycling at moderate current density for hundreds of hours (Figures S7 and S8, Supporting Information). In contrast, the symmetric cell in the E@EC/DEC cannot pass the test under harsh conditions and fails at 1 mA cm^{-2} because of short circuit.

The morphology of K metal plated on Al-C after the 1st and 10th discharging was characterized by atomic force microscopy (AFM) in an Ar-filled glovebox. The 3D topographic images in Figure 2d–g distinguish the height with different brightness, where the brighter color indicates the higher position. We utilize the average roughness of the surface, *Ra*, to evaluate the morphology of K metal plated.[20] As displayed in Figure 2d–g, the value of *Ra* is always lower in the E@1,3-DX. To present the morphology more clearly, we obtained the cross-sectional height profiles as well (Figures S9 and S10, Supporting Information). They demonstrate that the E@1,3-DX can lead to a more homogenous morphology of the deposited K metal. It probably arises from suppressed dendrite growth, explaining the better cycling stability of the K metal anode in the E@1,3-DX, as discussed above. Moreover, the morphology becomes flatter from the 1st to the 10th cycle in both electrolytes. This could be attributed to a more stable plating/stripping process due to the formation of a robust SEI after the first several cycles, giving rise to increased CEs after ten cycles. The morphology of K metal anodes was also probed through scanning electron microscopy (SEM), as shown in Figure S11 (Supporting Information). The morphology in the E@1,3-DX is uniform and compact, while that in the E@EC/DEC is more uneven and has many obvious cracks formed as indicated by the red arrows.

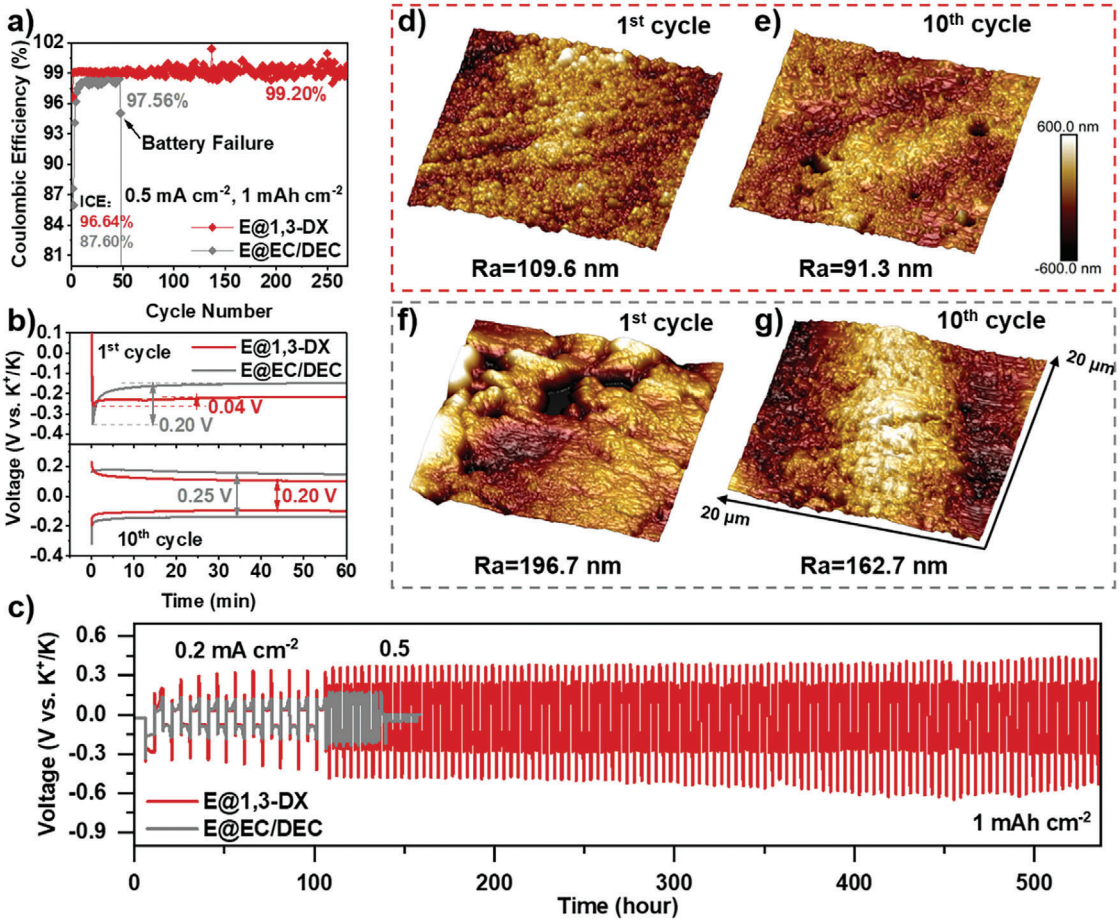

Figure 2. Electrochemical performance and morphology of K metal anode. a) CEs of K||Al-C cells in the two electrolytes. b) The nucleation process and the overpotential of K||Al-C cells in the 1st and 10th cycle at 0.5 mA cm^{-2}. c) Cycling performance of K||K symmetric cells in the E@1,3-DX and the E@EC/DEC at 0.2 mA cm^{-2} for the first 10 cycles, then at 0.5 mA cm^{-2} for the rest, with a fixed capacity of 1 mAh cm^{-2}. The AFM topographic images for the morphologies of K metal anodes cycled in d,e) the E@1,3-DX and f,g) the E@EC/DEC at the discharging state after d,f) the 1st and e,g) 10th cycle at 0.5 mA cm^{-2} for 1 mAh cm^{-2}.

2.4. Chemical Composition and Mechanical Properties of SEIs

To investigate the interfacial chemistry, X-ray photoelectron spectroscopy (XPS) was conducted to analyze the composition of SEIs on K metal anodes cycled in the E@1,3-DX and the E@EC/DEC. As shown in **Figure** 3a,b, the C content for the E@1,3-DX is lower than that for the E@EC/DEC. This suggests less decomposition of solvents in the E@1,3-DX because solvents are the only C source in both electrolytes. Meanwhile, the atomic concentrations of N, S, and F are higher in the SEI formed in the E@1,3-DX (Tables S4 and S5, Supporting Information), implying a more significant anion decomposition. The C—C/C—H and C-metal species in C 1s spectra could be ascribed to the decomposition of solvents to form organic species (Figure 3c).[15,21] These two kinds of species are lower in the SEI formed in the E@1,3-DX in each depth, indicating that the E@1,3-DX has less undesirable solvent reactions compared to the E@EC/DEC. The reason lies in the elevated proportion of anions in the solvation structure.

It is worth noticing that the F content on the surface of SEI in the E@1,3-DX is higher, which is reported to benefit the electrochemical cycling stability.[22] In terms of F 1s spectra, all the F-containing species originate from the decomposition of anion (Figure S12, Supporting Information). There are more S-F, K-F and less C-F species in SEIs formed in the E@1,3-DX. S-F and K-F species could be assigned to the inorganic reduction products of FSI^-. Specifically, K-F peaks are from potassium fluoride (KF). Detailed analysis in Figure 3d shows KF in the E@1,3-DX is more than that in the E@EC/DEC in each depth, whilst the percentage of KF in the whole SEI is growing with the sputtering time. Besides that, the O 1s XPS depth profiles were also analyzed (Figure S13a, Supporting Information). S = O peak could be assigned to the reduction products of FSI^-, and it is always more in the E@1,3-DX. The potassium oxide (K_2O) is also detected in the O 1s spectra with a higher amount in the E@1,3-DX (Figure S13b, Supporting Information). These inorganic species usually possess higher ionic conductivity, promoting the diffusion of K^+ through SEIs, regulating the deposition of K metal and suppressing dendrite growth.[4b,23]

The mechanical properties of SEIs formed in the two electrolytes were probed by AFM to explore the reason for the distinct CE, as SEI failure is one of the major reasons for the poor CE. In general, the two mechanical parameters used mostly are

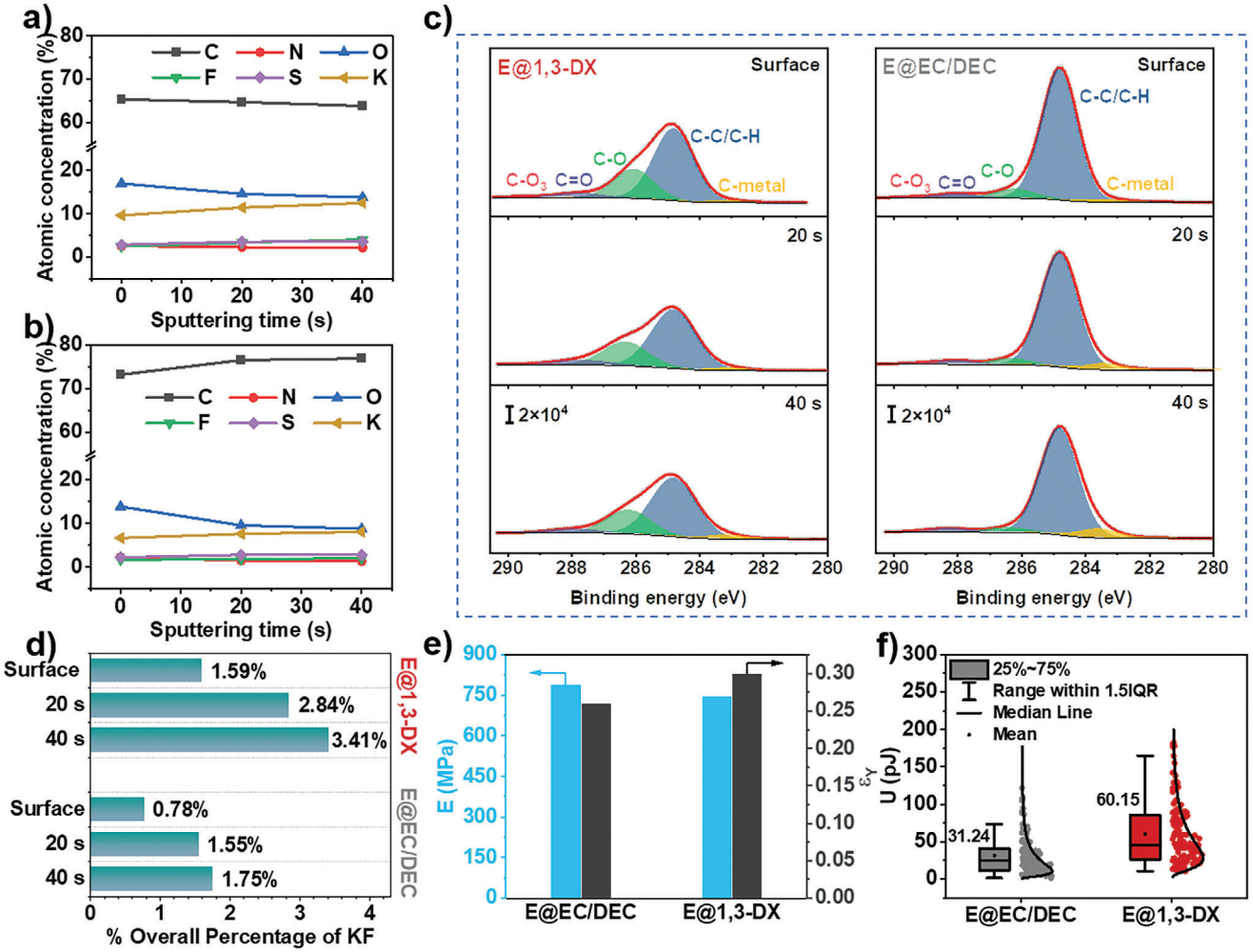

Figure 3. Chemical composition and mechanical properties of SEIs formed in the E@1,3-DX and the E@EC/DEC. Atomic concentrations at different depths of SEIs formed in a) the E@1,3-DX and b) the E@EC/DEC. c) C 1s XPS depth profiles of K metal anodes cycled ten times in the E@1,3-DX and the E@EC/DEC. d) The percentages of KF in overall SEI at different depths in two systems. e) Average Young's modulus E and elastic strain limit ϵ_Y of SEIs formed in the E@EC/DEC and the E@1,3-DX. f) The distributions and averages of U for different SEIs.

Young's modulus (E) and the elastic strain limit (ϵ_Y), to evaluate the mechanical stability of SEIs. The maximum elastic deformation energy (U), an energy-based concept combining the effects from these two parameters, is applied to characterize the capability of SEIs in accommodating the deformations.[24] A two-step consecutive nanoindentation test was conducted on AFM to obtain E, ϵ_Y, and U. More than 120 testing positions were collected for each sample to guarantee accuracy. As shown in Figure 3e, the SEI formed in the E@EC/DEC has a larger E, while that in the E@1,3-DX has a larger ϵ_Y. It could be elucidated by the chemical composition of the SEIs. It should be pointed out that although we focused on inorganic species during the XPS analysis, the main composition of two SEIs is organics, as evidenced by the high percentage of C content (Tables S4 and S5, Supporting Information).[20] The SEI formed in ether-based electrolytes tends to generate more polymer-like or oligomer-like species, while that in carbonate-based electrolytes would be dominated by species such as organic/inorganic carbonates.[25] Thus, the matrix of the SEI in the E@1,3-DX has higher elasticity than that in the E@EC/DEC despite the higher amount of inorganic species in the former. We calculated the value of U and plotted its distribution for two systems to reflect the mechanical stability of their SEIs (Figure 3f). The SEI formed in the E@1,3-DX possesses an average U of 60.15 pJ, which is almost twice that of the E@EC/DEC (31.24 pJ). Thus, the integrity of SEIs could be greatly maintained during charging/discharging in the E@1,3-DX, realizing a better K metal anode with a longer lifetime.

2.5. Oxidation Stability of Electrolytes and Full Cell Performance

Along with benefiting the anode, the electrolyte should also have a high oxidation stability for pairing with a high-voltage cathode. Linear sweep voltammetry (LSV) was carried out to study the electrochemical stability of the two electrolytes. As depicted in **Figure** 4a, the anodic current increases rapidly in the E@EC/DEC from 4.23 V, while the onset oxidation potential is 4.83 V under the E@1,3-DX. The high oxidation stability of the E@1,3-DX

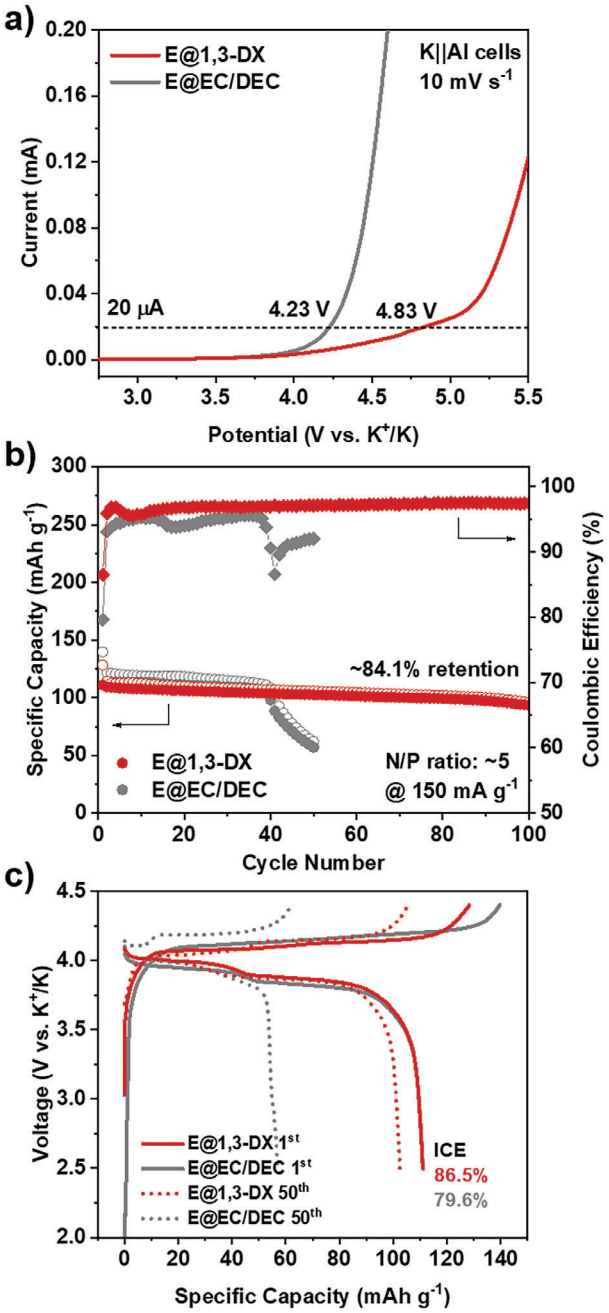

Figure 4. Oxidation stability of electrolytes and performances of full cells in the two electrolytes. a) LSV curves for K||Al cells in the E@1,3-DX and the E@EC/DEC, at the scan rate of 10 mV s^{-1}, from open circuit voltage to 5.5 V. b) The cycling performances of full cells in the E@1,3-DX and the E@EC/DEC, with the N/P ratio of 5, under the current density of 150 mA g^{-1} (based on the weight of the cathode). c) Charging/discharging curves for the 1st and the 50th cycles of the full cells in Figure 4b.

partly resolves the concerns of applying the diluted ether-based electrolytes in high-voltage PMBs to realize exceptional energy density.

A high-voltage Prussian Blue analogue $K_xMn[Fe(CN)_6]\cdot y(H_2O)$ (KMF) cathode was adopted to couple with K metal anode under the two electrolytes. The KMF possesses monoclinic phase with a particle size of ≈50 nm, as characterized by X-ray diffraction (XRD) and SEM (Figures S14 and S15, Supporting Information). We first collected the performance of K||KMF cells with excess K metal (Figure S16, Supporting Information). The cell with the E@1,3-DX presents an attractive CE of over 99%. Furthermore, Figure 4b shows the cycling performance of full cells in the E@1,3-DX and the E@EC/DEC with a negative/positive (N/P) capacity ratio of 5. The cell in the E@EC/DEC could only maintain for ≈40 cycles before a sudden capacity drop occurs. In sharp contrast, the full cell in the E@1,3-DX could work stably over 100 cycles, with a decent capacity retention of 84.1%. In addition, the cell with the E@1,3-DX possesses an ICE of 86.5% compared to 79.6% under the E@EC/DEC (Figure 4c), accompanied by a slightly lower polarization. These outcomes reveal the superiority of the E@1,3-DX used in full cells of PMBs, which originates from its compatibility with both anode and high-voltage cathode. It is worth mentioning that such stability cannot be achieved in widely used linear ether electrolytes, like DME, which shows a fatal overcharging within several cycles (Figure S17, Supporting Information). As for the rate performance (Figure S18, Supporting Information), the K||KMF cell in the E@1,3-DX delivers a specific capacity over 100 mAh g^{-1} under 4 C, and ≈90 mAh g^{-1} even under 10 C. Meanwhile, the cell shows a decent stability at both 0 and 60 °C (Figure S19, Supporting Information).

To study the chemical compositions of cathode-electrolyte interphases (CEIs) formed in the two electrolytes, the KMF cathodes after ten cycles in K||KMF cells were analyzed via XPS. As shown in Tables S6 and S7 (Supporting Information), the F content in the CEI formed in the E@1,3-DX is almost 1.7 times that in the E@EC/DEC on the surface, while it is over two times at the deeper layer. The advantage of the F content has been corroborated to be beneficial to the stability of CEIs under high voltage.[26] Moreover, the S content is also higher in the CEI formed in the E@1,3-DX, implying the decomposition of anion is promoted. The F 1s XPS depth profiles were also analyzed in Figure S20 (Supporting Information). These species are all from the decomposition of the anion FSI^-. K-F and S-F could be assigned to inorganics and they are obviously more in the CEI formed in the E@1,3-DX, revealing its inorganic-rich feature. These observations suggest unique advantages of the cyclic ether solvent, 1,3-DX, in concurrently stabilizing the K metal anode and satisfying the high-voltage cathode. Despite this, further efforts are required to address the low flash point of the solvent and high-temperature stability of the cell through continuous optimization the electrolyte formulations.

3. Conclusion

In summary, we reported a novel WSE, the E@1,3-DX, consisting of a solo salt and a solo non-fluorinated cyclic ether solvent, realizing high-performance PMBs under low concentration. Owing to the weak solvation ability of the 1,3-DX, the solvation structure of the E@1,3-DX is anion-dominated, manifested by the higher proportions of CIPs and AGGs. Therefore, the decomposition of anions is promoted, leading to the formation of inorganic-rich SEIs on the K metal anode. Meanwhile, the mechanical properties of SEIs are decent as well, with the deformation energy value almost twice that under the conventional carbonate electrolyte, contributing to maintain the integrity of SEIs during cycling.

Thus, the K metal anode cycled in the E@1,3-DX delivers an attractive average CE of 99.20% and a lifetime of 1300 h. In addition, the E@1,3-DX also possesses competitive oxidation stability. Consequently, an exceptional electrochemical performance has been achieved in K||KMF full cells, with stable cycling over 100 cycles and capacity retention of 84.1% at harsh conditions. This work provides a new WSE formula for advanced PMBs by stabilizing electrode-electrolyte interfaces, whilst this method can be extended to other novel metal/ion batteries as well.

4. Experimental Section

Materials: Potassium bis(fluorosulfonyl)imide (KFSI) (> 95.0%) was purchased from TCI CO., LTD, and was used without further treatment. 1,3-Dioxane (1,3-DX) (98%) was purchased from Macklin Inc. Ethylene carbonate (EC) and diethyl carbonate (DEC) were both purchased from DoDochem. EC/DEC mixed solvent was prepared by mixing these two solvents with a volume ratio of 1:1. KFSI was dissolved into 1,3-DX and EC/DEC with a concentration of 1 M. The solutions were prepared in a glovebox via magnetic stirring until dissolution. All the electrolytes used were dried with molecular sieves (3Å) over 24 h before usage. K metal (98%) was purchased from Sigma–Aldrich. For the preparation of $K_xMnFe(CN)_6{\cdot}yH_2O$ (KMF), manganese chloride ($MnCl_2$), potassium citrate, and potassium chloride (KCl) were purchased from Sigma-Aldrich. Potassium hexacyanoferrate(II) trihydrate ($K_4Fe(CN)_6{\cdot}3H_2O$) was purchased from Alfa Aesar. Polyvinylpyrrolidone (PVP, MW = 1300000) was purchased from IL USA.

Cathode Preparation: The KMF cathode was synthesized by precipitation in an aqueous solution. Solution A was obtained by dissolving 0.2568 g $MnCl_2$ and 0.35235 g potassium citrate into 20 mL deionized (DI) water. Solution B was obtained from the dissolution of 1.437 g $K_4Fe(CN)_6{\cdot}3H_2O$, 7.12 g KCl, and 0.111 g PVP into 40 mL DI water. Solution B was heated to 85 °C, while solution A was maintained at room temperature. Then Solution A was added dropwise into Solution B at 60 °C within 30 min. The magnetic stirring was continued for another 3 h, and an aging process lasting for 1 h was required. The precipitation was then collected by centrifugation and dried in a vacuum oven at 100 °C.

Electrode Preparation: KMF powder was ground with conductive carbon black Super P (Saibo Electrochemical Materials Co., Ltd.) and the binder sodium carboxymethyl cellulose (CMC) (Sigma-Aldrich) by a mass ratio of 6:3:1 in an agate mortar. Then, a certain amount of DI water was added to obtain a homogenous slurry via magnetic stirring overnight. The slurry was then blade coated onto a carbon-coating Al (Al-C) foil and was dried under vacuum at 80 °C for >12 h. It was cut into discs with a diameter of 12.5 mm. The weight of active material in each KMF electrode was ≈1.5 mg. For K||Al-C cells, the Al-C foil was cut into discs with a diameter of 12 mm. Given the merits of low cost and the anti-corrosion ability, Al-C is used as current collectors. K metal anode was prepared by rolling, which was punched into a disc with a diameter of 12 mm. For K||KMF full cells with the N/P ratio, based on the capacity of KMF cathode, a certain amount of K was electrochemically deposited on the Al-C current collector.

Electrochemical tests: CR2032 type K||Al-C, K||K, K||KMF and full cells were all assembled in a glovebox with water and oxygen levels below 0.1 ppm. K||Al-C cell used a separator group of GF/D-Celgard 2325, while K||K utilized a sandwich-type separator group as Celgard-GF/D-Celgard to reduce the possibility of short circuit. Except for full cells with a certain capacity ratio, the K metal anodes were excessive. As for electrolyte dosage, in the K||K cells, 150 µL electrolyte was added. Other cells contained ≈80 µL electrolyte.

Characterization: The solvation structure of electrolytes was studied with a Bruker 600 MHz Nuclear magnetic resonate (NMR) spectroscopy and a confocal Raman microscopy (Witec alpha 300 R) using a laser of 532 nm. The C atom was chosen to conduct NMR testing because of its suitable spin quantum number and the much higher natural abundance than O. The external reference for ^{13}C NMR is dimethyl sulfoxide (DMSO) with a chemical shift at 39.96 ppm, while that for ^{19}F NMR is 0.1 M fluorobenzene/deuterated chloroform ($CDCl_3$), at −112.98 ppm. The NMR peaks for different C atoms in the 1,3-DX are distinguished by referring to SDBSWeb: https://sdbs.db.aist.go.jp (National Institute of Advanced Industrial Science and Technology, 2023). The morphology of K metal anode and the mechanical properties of SEIs were characterized by atomic force microscopy (AFM) (Bruker Dimension Icon, Santa Barbara, CA, USA) located in an Ar-filled glovebox. The probe employed is antimony-doped silicon (RTESPA-300, Bruker), with a spring constant of 18.80 N m^{-1}, a deflection sensitivity of 99.50 nm V^{-1} (calibrated on a clean sapphire sample), and a tip radius of 12.50 nm (acquired from a reference sample with a known elastic modulus). Detailed testing methods could be found in the previous work.[20,24] The interfacial chemistry of the cycled K metal anode was investigated by X-ray photoelectron spectroscopy (XPS) (Thermo Fisher Scientific Nexsa). The electrodes disassembled in the glovebox were rinsed with respective solvents and dried before further transfer. To avoid contamination, all the samples were transferred via an Ar-filled container sealed in the glovebox. Linear sweep voltammetry (LSV) was performed on a Bio-Logic SAS SP-150 workstation (France) with a scan rate of 10 mV s^{-1}, from the open circuit voltage to 5.5 V (vs K^+/K), to test the oxidation stability. The working electrode was pure Al foil with a diameter of 19 mm, and the counter and reference electrodes were both K metal foil. To better quantify the onset oxidation voltage, the voltage value corresponding to the anodic current as 20 µA was recorded.[10] X-ray diffraction (XRD) of pristine KMF powder was tested on the Rigaku Smartlab 9kW-Advance X-ray diffractometer. The morphology information of KMF powder was gained from ultra-high resolution scanning electron microscopy (TESCAN MAIA3).

Supporting Information

Supporting Information is available from the Wiley Online Library or from the author.

Acknowledgements

The authors would like to express their sincere thanks to the financial support from the Research Institute for Advanced Manufacturing (RIAM) of The Hong Kong Polytechnic University (project code: 1-CDJU). The work described in this paper was substantially supported by a grant from the NSFC/RGC Joint Research Scheme sponsored by the Research Grants Council of Hong Kong and the National Natural Science Foundation of China (Project No. N_PolyU584/23).

Conflict of Interest

The authors declare no conflict of interest.

Data Availability Statement

The data that support the findings of this study are available from the corresponding author upon reasonable request.

Keywords

cyclic ether, interfacial chemistry, mechanical properties, potassium metal batteries, weakly solvating electrolytes

Received: May 6, 2024
Revised: July 7, 2024
Published online: August 8, 2024

[1] a) X. Min, J. Xiao, M. Fang, W. Wang, Y. Zhao, Y. Liu, A. M. Abdelkader, K. Xi, R. V. Kumar, Z. Huang, *Energy Environ. Sci.* **2021**, *14*, 2186; b) W. Xu, H. Wang, J. Hu, H. Zhang, B. Zhang, F. Kang, D. Zhai, *Chem. Commun.* **2021**, *57*, 1034; c) C. Wei, Y. Tao, H. Fei, Y. An, Y. Tian, J. Feng, Y. Qian, *Energy Storage Mater.* **2020**, *30*, 206.
[2] J. Hu, H. Wang, S. Wang, Y. Lei, L. Qin, X. Li, D. Zhai, B. Li, F. Kang, *Energy Storage Mater.* **2021**, *36*, 91.
[3] a) R. Rajagopalan, Y. Tang, X. Ji, C. Jia, H. Wang, *Adv. Funct. Mater.* **2020**, *30*, 1909486; b) W. Li, D. Wang, Z. Gong, X. Guo, J. Liu, Z. Zhang, G. Li, *Carbon* **2020**, *161*, 97.
[4] a) N. Xiao, W. D. McCulloch, Y. Wu, *J. Am. Chem. Soc.* **2017**, *139*, 9475; b) H. Wang, J. Dong, Q. Guo, W. Xu, H. Zhang, K. C. Lau, Y. Wei, J. Hu, D. Zhai, F. Kang, *Energy Storage Mater.* **2021**, *42*, 526.
[5] H. Wang, J. Hu, J. Dong, K. C. Lau, L. Qin, Y. Lei, B. Li, D. Zhai, Y. Wu, F. Kang, *Adv. Energy Mater.* **2019**, *9*, 1902697.
[6] a) P. Liu, D. Mitlin, *Acc. Chem. Res.* **2020**, *53*, 1161; b) Y. Lei, D. Han, J. Dong, L. Qin, X. Li, D. Zhai, B. Li, Y. Wu, F. Kang, *Energy Storage Mater.* **2020**, *24*, 319.
[7] a) Y. X. Yao, X. Chen, C. Yan, X. Q. Zhang, W. L. Cai, J. Q. Huang, Q. Zhang, *Angew. Chem., Int. Ed.* **2021**, *60*, 4090; b) Y. Zhao, T. Zhou, D. Baster, M. El Kazzi, J. W. Choi, A. Coskun, *ACS Energy Lett.* **2023**, *8*, 3180; c) H. Wang, D. Yu, X. Wang, Z. Niu, M. Chen, L. Cheng, W. Zhou, L. Guo, *Angew. Chem., Int. Ed.* **2019**, *131*, 16603.
[8] Z. Wang, B. Zhang, *Energy Mater. Devices* **2023**, *1*, 9370003.
[9] a) S. Chen, J. Zheng, D. Mei, K. S. Han, M. H. Engelhard, W. Zhao, W. Xu, J. Liu, J. G. Zhang, *Adv. Mater.* **2018**, *30*, 1706102; b) X. Ren, S. Chen, H. Lee, D. Mei, M. H. Engelhard, S. D. Burton, W. Zhao, J. Zheng, Q. Li, M. S. Ding, M. Schroeder, J. Alvarado, K. Xu, Y. S. Meng, J. Liu, J.-G. Zhang, W. Xu, *Chem* **2018**, *4*, 1877.
[10] S. Li, H. Zhu, C. Gu, F. Ma, W. Zhong, M. Liu, H. Zhang, Z. Zeng, S. Cheng, J. Xie, *ACS Energy Lett.* **2023**, *8*, 3467.
[11] J. Li, Y. Hu, H. Xie, J. Peng, L. Fan, J. Zhou, B. Lu, *Angew. Chem., Int. Ed.* **2022**, *61*, e202208291.
[12] a) C. Li, R. D. Guha, A. Shyamsunder, K. A. Persson, L. F. Nazar, *Energy Environ. Sci.* **2024**, *17*, 190; b) Y. Wang, R. Xu, B. Xiao, D. Lv, Y. Peng, Y. Zheng, Y. Shen, J. Chai, X. Lei, S. Luo, X. Wang, X. Liang, J. Feng, Z. Liu, *Mater. Today Phys.* **2022**, *22*, 100620.
[13] L. Yang, A. Xiao, B. L. Lucht, *J. Mol. Liq.* **2010**, *154*, 131.
[14] a) Y. Wang, Z. Cao, Z. Ma, G. Liu, H. Cheng, Y. Zou, L. Cavallo, Q. Li, J. Ming, *ACS Energy Lett.* **2023**, *8*, 1477; b) D. Guo, J. Wang, T. Lai, G. Henkelman, A. Manthiram, *Adv. Mater.* **2023**, *35*, 2300841.
[15] Z. Wang, C. Chen, D. Wang, Y. Zhu, B. Zhang, *Angew. Chem., Int. Ed.* **2023**, *62*, e202303950.
[16] M. Shimizu, T. Koya, A. Nakahigashi, N. Urakami, T. Yamakami, S. Arai, *J. Phys. Chem. C* **2020**, *124*, 13008.
[17] S. Liu, J. Mao, Q. Zhang, Z. Wang, W. K. Pang, L. Zhang, A. Du, V. Sencadas, W. Zhang, Z. Guo, *Angew. Chem., Int. Ed.* **2020**, *59*, 3638.
[18] S. Wu, J. Hwang, K. Matsumoto, R. Hagiwara, *Adv. Energy Mater.* **2023**, *13*, 2302468.
[19] B. D. Adams, J. Zheng, X. Ren, W. Xu, J.-G. Zhang, *Adv. Energy Mater.* **2018**, *8*, 1702097.
[20] Y. Gao, Z. Hou, R. Zhou, D. Wang, X. Guo, Y. Zhu, B. Zhang, *Adv. Funct. Mater.* **2022**, *32*, 2112399.
[21] M. Jiang, Q. Zhang, D. L. Danilov, R.-A. Eichel, P. H. L. Notten, *ACS Appl. Energy Mater.* **2021**, *4*, 10333.
[22] X. Fan, L. Chen, O. Borodin, X. Ji, J. Chen, S. Hou, T. Deng, J. Zheng, C. Yang, S. C. Liou, K. Amine, K. Xu, C. Wang, *Nat. Nanotechnol.* **2018**, *13*, 715.
[23] Y. Zhao, T. Zhou, L. P. H. Jeurgens, X. Kong, J. W. Choi, A. Coskun, *Chem* **2023**, *9*, 682.
[24] Y. Gao, X. Du, Z. Hou, X. Shen, Y.-W. Mai, J.-M. Tarascon, B. Zhang, *Joule* **2021**, *5*, 1860.
[25] J. Huang, X. Guo, X. Du, X. Lin, J.-Q. Huang, H. Tan, Y. Zhu, B. Zhang, *Energy Environ. Sci.* **2019**, *12*, 1550.
[26] H. Tan, D. Zhai, F. Kang, B. Zhang, *Carbon* **2021**, *178*, 363.